Model Predictive Current Control with Inherent Damping for Inverters Under Weak Grid Conditions

Seungyong Lee and Roy McCann
University of Arkansas, Fayetteville AR, USA

***Abstract*—Increased capacity associated with renewable energy sources has created a need for improved methods for controlling power flows from inverter-based generation. This research provides a comparative study of finite-control-set model predictive current control (FCS-MPC-based) with respect to conventional proportional-integral-based (PI-based) synchronous current control for a three-phase voltage source inverter (VSI). The inverter is accompanied by an inductive-capacitive-inductive (LCL) filter to attenuate pulse width modulation (PWM) switching harmonics. However, an LCL filter introduces a resonance near to the control stability boundary, giving rise to substantial complexity from a control perspective. In order to avoid potential instability caused by the resonance, active damping can be included in the PI-based current control. Though properly designed active damping can improve inverter stability, in practice the robustness of standard PI control is not attainable due to variability in the grid inductance at the point of common coupling (PCC). This is due to impedance variations causing large shifts in the LCL resonance frequency. Weak grid conditions (i.e., a low short-circuit ratio) and a correspondingly high line impedance are particularly susceptible to LCL induced resonance instabilities. As an approach to operate with grid impedance variations and weak grid conditions, FCS-MPC has the potential to produce superior performance compared to PI-based current control methods. This comparative study indicates that FCS-MPC has improved resonance damping and fast dynamic capability in a system with renewable energy sources under weak grid conditions. Detailed results from MATLAB/SimPower are presented to validate the suggested FCS-MPC method where it is robust to uncertainty in the grid impedance variations. Overall results indicate an improvement over conventional PI-based current control methods.**

***Index Terms*—Model predictive control, resonance frequency, weak grids, three-phase voltage source inverter.**

I. INTRODUCTION

As use of renewal resources rises, the number of grid-connected inverters increases in power grid. The inverter is accompanied by an inductive-capacitive-inductive (LCL) filter to attenuate the pulse width modulation (PWM) switching harmonics. The filter enables to reduce overall size and weight when compared with a conventional inductive (L) filter [1-5]. However, LCL filters introduce substantial complexity from a control perspective due to a resonance phenomenon caused by the filter elements which creates a pair of system poles located on the closed-loop stability boundary. Therefore, designing a control system for a grid-connected voltage source inverter (VSI) with an LCL filter is a very challenging task [6-8]. In particular, a weak grid implying a grid with a lower short circuit ratio (SCR) can lead to voltage fluctuations at the inverter terminals and consequently cause inverter instability [9-13]. The literature [8] demonstrates a decrease in the grid inductance does not necessarily improve the stability of grid-connected VSIs. It also claims that the system stability is a function of both the grid R/X ratio and grid inductance. Additionally, despite the grid-side inductor of the LCL filter is in series with the grid impedance, they have different effects on the stability of the system [14].

There are many types of model predictive control (MPC) under different names but they all have a similarity, which is to predict future events and take control actions based on objective function minimization [15–17]. Since predictive control drew a growing attention almost three decades ago, research and development activities in finite control set MPC (FCS-MPC) have become substantially active for the last decade [17], [18]. As the consequences of the intensive study, advanced analysis techniques and practical tests for FCS-MPC have been performed for a wide range of power conversion applications [16]. FCS-MPC has many advantages over classical linear controller, which are nonlinear nature, modulator-free structure and high-performance operation [17], [19]. These merits suggest that FCS-MPC could be applied in a wide variety of systems in place of conventional control methods which are quite vulnerable to uncertainties in practice [17], [20-22]. Non-linearity of systems limits the closed-loop performance because the conventional methods develop controllers based on a linearized model [17].

For a grid-connected VSI, current control is commonly performed with a linear PI controller in the synchronous reference frame. A controller has been designed based on the fixed resonant frequency of an output LCL filter. However, the filter resonance is also affected by the equivalent grid impedance and is therefore subject to change depending on grid conditions. This further complicates designing a robust PI controller. As a solution of the issue, FCS-MPC with a cost function including a term which tracks the derivative of capacitor voltage reference is designed and applied to a weak grid-connected VSI. Performances between PI-based current control and FCS-MPC are compared from active damping perspective [23].

II. SYSTEM MODEL

I. PI-PWM CONTROL STRATEGY

Fig. 1 shows the general structure of a voltage source inverter (VSI) feeding current into a grid through an LCL output filter. The primary control goal for the system is to regulate the grid current i_2 to control the injected power into the grid. Typically, it is claimed that a single-loop feedback control is not adequate for this role because LCL-filter resonance causes controller instability [1], [7]. Fig. 2(a) shows such a single-loop feedback controller which is modeled in the z-domain to account for digital sampling. It is shown in Fig. 2(b) that a typical dual-loop control system that describes the resonance stability issue by including the active damping feedback of the capacitor current $i_c(z)$ via a damping gain K [8]. For both of these controllers, $i_2^*(z)$ is the commanded grid current, $i_2(z)$ is the measured grid current, $G_c(z)$ is the controller transfer function, and the inverter is modeled as a linear V_{DC} gain, with a sample delay z^{-1} to take into account PWM transport delay [8]. For analysis of the control systems of Fig. 2 the discrete time-transfer functions for the LCL filter of $G_{i2}(z)$, $G_{ic}(z)$, and $i_2(z)/i_c(z)$ are required. The first two of these transfer functions are well described in the literature [1], [2] in the s-domain as

$$G_{i_2}(s) = \frac{i_2(s)}{V_o(s)} = \frac{1}{sL_1}\frac{\Upsilon_{LC}^2}{(s+\omega_{\text{res}}^2)} \tag{1}$$

$$G_{i_c}(s) = \frac{i_c(s)}{V_o(s)} = \frac{1}{sL_1}\frac{s^2}{(s+\omega_{\text{res}}^2)} \tag{2}$$

where $\omega_{\text{res}} = \sqrt{(L_1+L_2)/(L_1L_2C_f)}$ and $\gamma_{LC} = \sqrt{1/(L_2C_f)}$. It is important to note that winding resistance and core loss of the inductors have been neglected in (1) and (2). With the associated resistance neglected, the system represents the worst undamped case, which highlights a resonance stability issue [8]. The third transfer function relating i_2 to i_c can be obtained by taking the ratio of (1) and (2), i.e.,

$$\frac{i_2(s)}{i_c(s)} = \frac{G_{i_2}(s)}{G_{i_c}(s)} = \frac{\gamma_{LC}^2}{s^2}. \tag{3}$$

Applying the zero-order-hold (ZOH) transform to (1) and (2) with a sampling period of $T = 1/f_{\text{samp}}$ yields z-domain LCL filter transfer functions for i_2 and i_c.:

$$G_{i_2}(z) = \frac{i_2(z)}{V_o(z)} = \frac{T}{(L_1+L_2)(z-1)} - \frac{\sin(\omega_{\text{res}}T)}{\omega_{\text{res}}(L_1+L_2)} \times \frac{z-1}{z^2-2z\cos(\omega_{\text{res}}T)+1} \tag{4}$$

$$G_{i_c}(z) = \frac{i_c(z)}{V_o(z)} = \frac{\sin(\omega_{\text{res}}T)}{\omega_{\text{res}}L_1} \times \frac{z-1}{z^2-2z\cos(\omega_{\text{res}}T)+1}. \tag{5}$$

To discretize (3), it should be recognized that the grid current in Fig. 2(b) results from the cascaded connection of $G_{ic}(z)$ and $i_2(z)/i_c(z)$. Since the grid and capacitor currents are practically sampled at the same time instant, the delay attributed to this process is accounted for by the ZOH transformation. Hence, $i_2(s)/i_c(s)$ is discretized using an impulse-invariant transformation [8], so that no additional delay is introduced to the system model, yielding

$$\frac{i_2(z)}{i_c(z)} = \frac{\gamma_{LC}^2 T^2 z}{(z-1)^2}. \tag{6}$$

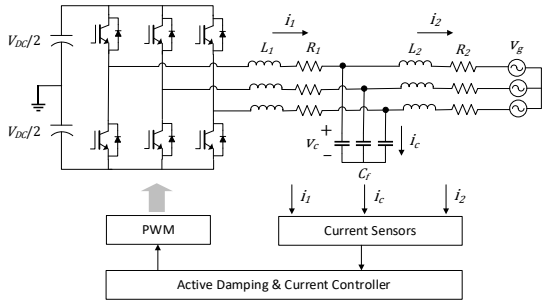

Fig. 1. Block diagram of the proposed model predictive current control scheme with the optimal state estimator.

TABLE. 1. System and control parameters.

Symbols	Parameters	Values
V_{DC}	DC supply voltage	800 V
	Grid phase/line-to-line voltage	277 V/480V
$L_1(R_1)$	Inverter-side inductance (internal resistance)	20 µH (3 mΩ)
$L_2(R_2)$	Grid-side inductance (internal resistance)	20 µH (3 mΩ)
C_f	Filter capacitance	1440 µF
F_{res}	L_1CL_2 resonant frequency	1320 Hz
Fs	Control sampling frequency	4 kHz

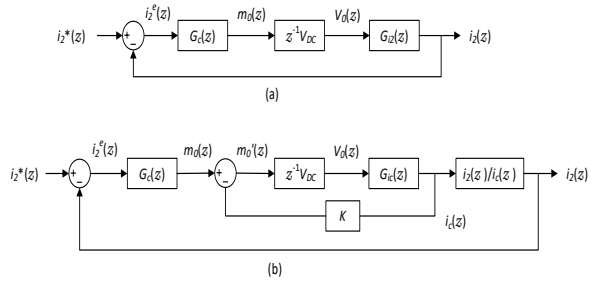

Fig. 2. Single-phase equivalent current controller architectures. (a) A single-loop feedback current controller. (b) Dual-loop controller with capacitor current active damping.

It is common to use a proportional plus resonance (PR) controller, which is equivalent to synchronous *dq*-frame proportional plus integral [3], to eliminate steady-state tracking errors at the fundamental frequency ω_o. The transfer function of the PR controller with the proportional gain K_p and resonant time constant T_r yields

$$G_c(s) = K_p\left(1 + \frac{1}{T_r}\frac{s}{(s^2+\omega_0^2)}\right). \tag{7}$$

The suitable discretization strategy for this controller is the Tustin transform with prewarping [8], which gives an equivalent discrete time controller transfer function of

$$G_c(z) = K_p\left(1 + \frac{1}{T_r}\frac{\sin(\omega_0 T)}{2\omega_0} \times \frac{z^2-1}{(z^2 - 2z\cos(\omega_0 T)+1)}\right). \tag{8}$$

These transfer functions can now be combined to yield open-loop forward-path expressions for the controllers of Fig. 2 so that control system analysis techniques, such as frequency response and root locus, can be utilized. For the single-loop controller shown in Fig. 2(a), the forward-path transfer function is readily obtained as

$$\frac{i_2(z)}{i_2^e(z)} = z^{-1}V_{\mathrm{DC}}G_c(z)G_{i_2}(z) \tag{9}$$

where $i_2^e(z) = i_2^*(z) - i_2(z)$ is the regulated current error. For the active damping controller shown in Fig. 2(b), first the analysis is carried out by closing the inner capacitor current feedback active damping loop, i.e.,

$$\frac{i_c(z)}{m_o(z)} = \frac{V_{\mathrm{DC}}G_{i_c}(z)}{z + KV_{\mathrm{DC}}G_{i_c}(z)}. \tag{10}$$

The forward-path transfer function of the overall system shown in Fig. 2(b) is obtained by combining this result with transfer functions (6) and (8), yielding

$$\begin{aligned}\frac{i_2(z)}{i_2^e(z)} &= G_c(z) \times \frac{i_c(z)}{m_o(z)} \times \frac{i_2(z)}{i_c(z)} \\ &= G_c(z) \times \frac{V_{\mathrm{DC}}G_{i_c}(z)[i_2(z)/i_c(z)]}{z + KV_{\mathrm{DC}}G_{i_c}(z)}.\end{aligned} \tag{11}$$

With the fact that the magnitude and phase contribution of the LCL filter resonance is insignificant at the crossover frequency, the system response is dominated by the series inductance. Hence the only low frequency component of the system model (4) is required, and the single loop forward-path transfer function reduces to

$$\angle\frac{i_2(z)}{i_2^e(z)} = z^{-1}V_{DC}K_p\frac{T}{(z-1)(L_1+L_2)}. \tag{12}$$

The proportional gain is then set to have unity gain at the desired crossover frequency using

$$K_p = \left|\frac{(L_1+L_2)(e^{j\omega_c T}-1)}{V_{DC}T}\right|. \tag{13}$$

With the approximation of $\left|e^{j\omega_c T}-1\right| \approx \omega_c T$, this gives

$$K_p \approx \frac{\omega_c(L_1+L_2)}{V_{DC}}. \tag{14}$$

A bounded range for damping gain *K* can be determined by using the critical resonant frequency$\omega = \pi/(3T)$, at which root loci stay on the unit circle, giving a maximum value for gain *K*. A minimum gain *K* can be found using Routh's stability criterion [8]. The maximum value of gain *K* can be obtained from the denominator of the closed loop transfer function by setting its magnitude is equal to unity. Substituting $G_{ic}(z)$ from (5) and $i_2(z)/i_c(z)$ from (6) gives

$$\left|\frac{V_{DC}\sin(\omega_{\mathrm{res}}T)}{\omega_{\mathrm{res}}L_1} \times \frac{K(z_0-1)^2 + K_p\gamma_{LC}^2 T z_0}{z_0(z_0-1)(z_0^2 - 2z_0\cos(\omega_{\mathrm{res}}T)+1)}\right| = 1 \tag{15}$$

where z_0 is a specific pole location on the root locus at which the magnitude becomes one as the damping gain increases. $z_0 = 0.5 + j\sqrt{3}/2$ is selected from $z = e^{j\omega_c T}$ with $\omega_{\mathrm{crit}} = \pi/3T$ and substitution into (15) with some mathematical manipulation gives $K_{\max}$:

$$K_{\max} = \frac{\omega_{\mathrm{res}}L_1}{V_{DC}\sin(\omega_{\mathrm{res}}T)}|1 - 2\cos(\omega_{\mathrm{res}}T)| + K_p\gamma_{LC}^2T^2. \tag{16}$$

K_{min} can be found using the limiting ratio of proportional gain K_p to damping gain K from the Routh's stability criterion in [8], which is given as

$$\frac{K_p}{K} \leq \frac{L_1 + L_2}{L_1} \Rightarrow K_{\min} = \frac{K_p L_1}{L_1 + L_2}. \quad (17)$$

Within these limits for the damping gain, a root locus pole placement strategy can be used to determine the value of K which achieves the most damping.

II. FCS-MPC STRATEGY

The dc-link voltage v_{dc}, the grid voltages v_{ga}, v_{gb}, and v_{gc} and the grid currents i_{2a}, i_{2b}, and i_{2c} are measured for the feedback control of the FCS-MPC. The dynamics of the grid-connected inverter is represented in the state-space as follows:

$$\dot{x}(t) = Ax(t) + B_i u_i(t) + B_g u_g(t)$$

$$y = Cx(t)$$

$$A := \begin{bmatrix} \frac{R_i}{-L_i} & 0 & 0 & 0 & \frac{1}{-L_i} & 0 \\ 0 & \frac{R_i}{-L_i} & 0 & 0 & 0 & \frac{1}{-L_i} \\ 0 & 0 & \frac{R_g}{-L_g} & 0 & \frac{1}{L_g} & 0 \\ 0 & 0 & 0 & \frac{R_g}{-L_g} & 0 & \frac{1}{L_g} \\ \frac{1}{C} & 0 & \frac{1}{-C} & 0 & 0 & 0 \\ 0 & \frac{1}{C} & 0 & \frac{1}{-C} & 0 & 0 \end{bmatrix}$$

$$B_i := \begin{bmatrix} \frac{1}{L_i} & 0 & 0 & 0 & 0 & 0 \\ 0 & \frac{1}{L_i} & 0 & 0 & 0 & 0 \end{bmatrix}^{\mathrm{T}} K_{\alpha\beta} \quad (18)$$

$$B_g := \begin{bmatrix} 0 & 0 & \frac{1}{-L_g} & 0 & 0 & 0 \\ 0 & 0 & 0 & \frac{1}{-L_g} & 0 & 0 \end{bmatrix}^{\mathrm{T}} K_{\alpha\beta}$$

$$C := \begin{bmatrix} 0 & 0 & 0 & 0 & 0 & 0 \\ 0 & 0 & 0 & 0 & 0 & 0 \\ 0 & 0 & 1 & 0 & 0 & 0 \\ 0 & 0 & 0 & 1 & 0 & 0 \\ 0 & 0 & 0 & 0 & 0 & 0 \\ 0 & 0 & 0 & 0 & 0 & 0 \end{bmatrix}$$

$$K_{\alpha\beta} = \frac{2}{3} \begin{bmatrix} 1 & -\frac{1}{2} & -\frac{1}{2} \\ 0 & \frac{\sqrt{3}}{2} & -\frac{\sqrt{3}}{2} \end{bmatrix}$$

where $x = [i_{1\alpha} \quad i_{1\beta} \quad i_{2\alpha} \quad i_{2\beta} \quad v_{c\alpha} \quad v_{c\beta}]^{\mathrm{T}}$, u_i and u_g are the inverter output voltage and grid voltage vectors respectively. FCS-MPC consists of three main parts, which are extrapolation of reference current, prediction of state variables in discrete-time model, and cost function minimization. The finite number of switching state combinations is evaluated in terms of error between predictive currents and extrapolated reference currents by using the absolute cost function. A switching state corresponding to a minimum cost function value is applied to the inverter switches. The cost function used for the implementation is

$$g(k) = |\hat{\imath}^*(k+1) - \mathrm{i}^p(k+1)|. \quad (19)$$

The minimum cost function value is identified by comparison and the corresponding switching state combination is applied to the inverter. To improve steady-state performance of the control, a term which tracks the derivative of the capacitor voltage reference is added to the cost function and expressed as [24],

$$g_{der} = \left|C_f \omega_n v_{f\beta}^* - i_{1\alpha} + i_{2\alpha}\right| + \left|C_f \omega_n v_{f\alpha}^* + i_{1\beta} - i_{2\beta}\right| \quad (20)$$

where ω_n is the nominal angular grid frequency and v_f is the voltage of the capacitor. The term has an active damping effect and ensure robust performance in steady-state and dynamic response. This also allows for easy compensation of nonlinear effects.

III. SIMULATION

To assess the relationship between current controller stability and LCL filter resonant frequency, forward-path transfer functions for the single and dual-loop current controllers have been calculated using (9) and (11) for the system with the parameters given in Table I. The Bode plot of Fig. 3 shows frequency responses of the single- and dual-loop current controllers when the resonant frequency is lower than half the sampling frequency. Without active damping (i.e., single loop), the high-frequency LCL filter resonance at 8.3 krad/s causes a sharp phase transition through −180° with a very high resonant frequency magnitude. This is an unconditionally unstable situation for any available controller gains. Therefore, the resonant frequency magnitude should be damped such that the magnitude remains below 0 dB for ensuring stability of the system. Incorporating active damping using the dual-loop controller attenuates the resonant peak magnitude below zero magnitude, so that the system can be stabilized with the selected controller gain. There exists a critical LCL filter resonant frequency above which a single-loop controller could achieve a stable response, but below which active damping is required to ensure stability. If the LCL filter resonance frequency is above the critical frequency ω_{crit}, a single loop is sufficient for a stable system. However, stability does not depend solely on the resonance frequency of the LCL filter because the region of operation tends to alter

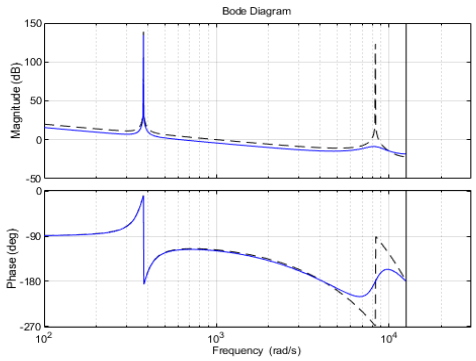

Fig 3. Bode plot of the forward-path transfer functions for the single- and dual-loop current controller. Root loci of dual-loop current controller with respect to active damping gain *K*.

based on grid conditions. In particular a weak grid has a significant effect on the resonance frequency with high impedance. In addition, insufficient damping must be taken into consideration for ensuring stability of the system. Apparently, there is a maximum damping gain, beyond which the system loss its stability. For the system with a sampling frequency of 4 kHz, a bounded range for damping gain K is determined from equations (16) and (17), which gives $K_{\min} \leq K \leq K_{\max}$ with $K_{\min} = 0.02$ A^{-1} and $K_{\max} = 0.1625$ A^{-1}. This means that the relatively limited range of damping gain allows for effective stability control. The best available value for the damping gain range is selected to place the two resonance poles as far from the unit circle as possible.

Simulation studies for the LCL-filtered VSI system with active damping applied are performed using Matlab/Simulink®. Power is raised at 0.2 s and then active damping is disabled at 0.4 s. The system in a stiff grid still demonstrates stable operation despite of resonance caused from the LCL filter. This is because that the filter resonant frequency is higher than the critical frequency.

For comparison, the same system is connected to a weak grid with impedance being thrice as high as that of the stiff grid. As soon as the active damping feedback is disabled, large resonant current occurs, which deteriorates stability of the system shown in Fig. 4 (b). The grid-connected VSI regulated by FCS-MPC is simulated for a comparison as shown in Fig 4 (c). Under a week grid condition, the FCS-MPC keeps the system from being affected by resonance. The term to track the derivative of capacitor voltage reference, which is added to the cost function, plays a role as active damping. Thereby it improves performances in steady-state and dynamic response.

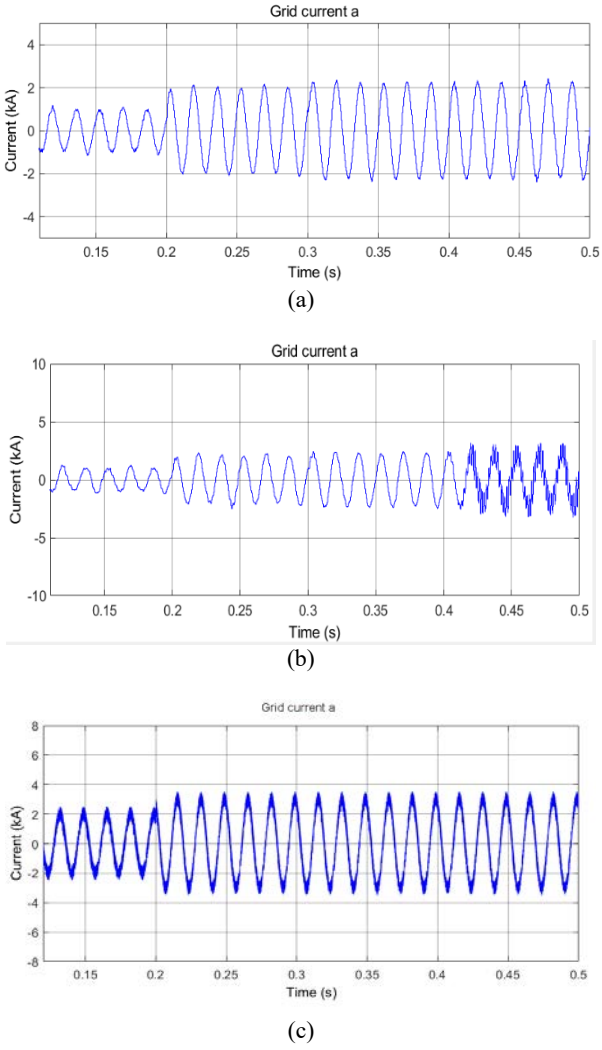

Fig. 4. (a) (b) PI current control of a VSI with an LCL filter with a step change in active power at 0.2 s and subsequent active damping off at 0.4 s in a stiff grid (a) and in a weak grid (b). (c) FCS-MPC of a VSI with an LCL filter with a step change in active power at 0.2 s in a weak grid.

IV. CONCLUSION

Applied active damping to the grid-connected VSI satisfactorily dampens out the resonance effect caused by an LCL filter. However, grid variations in impedance bring difficulties in designing PI control with optimal active damping. Therefore, an advanced control strategy, especially MPC is expected as a potential approach to robust controller design against complexity and instability caused by resonant current in a weak grid-connected three-phase inverter. This is due to the fact that high dynamic performances of the system can be achieved with the flexibility of the cost function in MPC design. A grid-connected VSI regulated by FCS-MPC demonstrates

good performances in terms of active damping and dynamic response in a weak grid condition. Thus, MPC is particularly expected to allow for easy compensation for the complicated LCL filter resonant frequency issue attributed to variations in grid condition.

REFERENCES

[1] J. Dannehl, F. W. Fuchs, S. Hansen, P. B. Thogersen, "Investigation of active damping approaches for PI-based current control of grid-connected pulse width modulation converters with LCL filters", IEEE Trans. Ind. Appl., vol. 46, no. 4, pp. 1509-1517, Jul./Aug. 2010.

[2] Y. Tang, P. C. Loh, P. Wang, F. H. Choo, F. Gao, "Exploring inherent damping characteristics of LCL-filters for three-phase grid-connected voltage source inverters", IEEE Trans. Power Electron., vol. 27, no. 3, pp. 1433-1443, Mar. 2012.

[3] D.G. Holms, T.A. Lipo, B.P. McGrath, W.Y. Kong, "Optimized design of stationary frame three phase ac current regulators", IEEE Trans. Power Electron., vol. 24, no. 11, pp. 2417-2426, Nov. 2009.

[4] G. Shen, Z. Xuancai, Z. Jun, X. Dehong, "A new feedback method for PR current control of LCL-filter-based grid-connected inverter", IEEE Trans. Ind. Electron., vol. 57, no. 6, pp. 2033-2041, Jun. 2010.

[5] W. Yao, Y. Yang, X. Zhang, F. Blaabjerg, P. C. Loh, "Design and analysis of robust active damping for LCL filters using digital notch filters", IEEE Trans. Power Electron., vol. 32, no. 3, pp. 2360-2375, Mar. 2017. J. Rodriguez et al. "Predictive current control of a voltage source inverter" IEEE Trans. Ind. Electron. vol. 54 no. 1 pp. 495-503 Feb. 2007.

[6] C. Bao, X. Ruan, X. Wang, W. Li, D. Pan, K. Weng, "Step-by-step controller design for LCL-type grid-connected inverter with capacitor-current-feedback active-damping", IEEE Trans. Power Electron., vol. 29, no. 3, pp. 1239-1253, Mar. 2014.

[7] J. Yin, S. Duan, B. Liu, "Stability analysis of grid-connected inverter with LCL filter adopting a digital single-loop controller with inherent damping characteristic", IEEE Trans. Ind. Informat., vol. 9, no. 2, pp. 1104-1112, May 2013.

[8] S. Parker, B. P. McGrath, D. G. Holmes, "Region of active damping control for LCL filters", IEEE Trans. Ind. Appl., vol. 50, no. 1, pp. 424-432, Jan./Feb. 2014.

[9] M. Liserre, R. Teodorescu, F. Blaabjerg, "Stability of photovoltaic and wind turbine grid-connected inverters for a large set of grid impedance values", IEEE Trans. Power Electron., vol. 21, no. 1, pp. 263-272, Jan. 2006.

[10] Y. Huang, X. Yuan, J. Hu, P. Zhou, "Modeling of VSC connected to weak grid for stability analysis of DC-link voltage control", IEEE J. Emerg. Sel. Topics Power Electron., vol. 3, no. 4, pp. 1193-1204, Dec. 2015.

[11] M. Ashabani, Y. A.-R. I. Mohamed, "Integrating VSCs to weak grids by nonlinear power damping controller with self-synchronization capability", IEEE Trans. Power Syst., vol. 29, no. 2, pp. 805-814, Mar. 2014.

[12] M. Davari, Y. A.-R. I. Mohamed, "Robust vector control of a very weak-grid-connected voltage-source converter considering the phase-locked loop dynamics", IEEE Trans. Power Electron., vol. 32, no. 2, pp. 977-994, Feb. 2017.

[13] D. Yang, X. Ruan, H. Wu, "Impedance shaping of the grid-connected inverter with LCL filter to improve its adaptability to the weak grid condition", IEEE Trans. Power Electron., vol. 29, no. 11, pp. 5795-5805, Nov. 2014.

[14] A. Adib, B. Mirafzal, X. Wang, F. Blaabjerg, "On stability of voltage source inverters in weak grids", IEEE Access, vol. 6, pp. 4427-4439, Jan. 2018.

[15] P. Cortes M. P. Kazmierkowski R. M. Kennel D. E. Quevedo J. Rodriguez "Predictive control in power electronics and drives" IEEE Trans. Ind. Electron. vol. 55 no. 12 pp. 4312-4324, Dec. 2008.

[16] K. S. Low R. Cao "Model predictive control of parallel-connected inverters for uninterruptible power supplies" IEEE Trans. Ind. Electron. vol. 55 no. 8 pp. 2884-2893, Aug. 2008.

[17] S. Vazquez et al. "Model predictive control: A review of its applications in power electronics" IEEE Ind. Electron. Mag. vol. 8 no. 1 pp. 16-31, Mar. 2014.

[18] V. Yaramasu and B. Wu, “Fundamentals of model predictive control,” in Model predictive control of wind energy conversion systems, Hoboken, New Jersey, USA: Wiley, 2016, pp. 117−148.

[19] J. Rodriguez et al. "State of the art of finite control set model predictive control in power electronics" IEEE Trans. Ind. Informat. vol. 9 no. 2 pp. 1003-1016, May 2013.

[20] S. Alepuz S. Busquets-Monge J. Bordonau J. Gago D. Gonzalez and J. Balcells "Interfacing Renewable Energy Sources to the Utility Grid Using a Three-Level Inverter" IEEE Trans. on Ind. Electron. vol. 53 no. 5 pp. 1504-1511, Oct. 2006.

[21] S. Kouro P. Cortes R. Vargas U. Ammann J. Rodriguez "Model predictive control—A simple and powerful method to control power converters" IEEE Trans. Ind. Electron. vol. 56 no. 6 pp. 1826-1838, Jun. 2009.

[22] J. Rodriguez et al. "Predictive current control of a voltage source inverter" IEEE Trans. Ind. Electron. vol. 54 no. 1 pp. 495-503, Feb. 2007.

[23] J. Nørgaard M. Graungaard T. Dragičević, F. Blaabjerg, "Current Control of LCL-Filtered Grid-Connected VSC using Model Predictive Control with Inherent Damping" in 2018 20th European Conference on Power Elctronics and Applications. EPE’s 18 ECCE Europe, pp.1-9, 2018.

[24] T. Dragicevic, "Model Predictive Control of Power Converters for Robust and Fast Operation of AC Microgrids", *IEEE Trans. Power Electron.*, vol. 33, no. 7, pp. 6304-6317, Jul. 2018.